JMEPEG (2009) 18:221–230
DOI: 10.1007/s11665-008-9268-7

1059-9495/$19.00

An Algorithm for Inverse Modeling of Layer-by-Layer Deposition Processes

S.G. Lambrakos and K.P. Cooper

(Submitted May 22, 2008)

Metallic parts can be made by deposition of liquid metal in a layer-by-layer fashion. By this means, layered structures can be produced that are made up of overlapping reinforced droplets. In particular, prototypes, i.e., customized parts and tooling, can be produced in this way. In order that layer-by-layer fabrication techniques transition from prototyping to manufacturing, however, the processes must be made reliable and consistent. Accordingly, detailed microstructural and thermal characterizations of the product are needed to advance manufacturing goals based on layer-by-layer deposition processes. The inherent complexity of layer-by-layer deposition processes, characteristic of energy and mass deposition processes in general, is such that process modeling based on theory, or the direct-problem approach, is extremely difficult. A general approach to overcoming difficulties associated with this inherent complexity is the inverse-problem approach. Presented here is an algorithm for inverse modeling of heat transfer occurring during layer-by-layer deposition, which is potentially adaptable for prediction of temperature histories in samples that are made by layer-by-layer deposition processes.

Keywords fabricated metal, machining, modeling processes

1. Introduction

Benefits of layer-by-layer manufacturing by direct deposition of metals or solid freeform fabrication are many. The ability to make spare or replacement parts on demand, to repair damaged parts, and to add features on existing parts are attractive advantages. There are many material-specific, layer manufacturing techniques. For metals, direct deposition techniques appear most suitable. Direct deposition involves building three-dimensional, net-shape metallic structures (Ref 1). A CAD solid model of the object or part is sliced into layers. Each slice or layer is formed by overlapping several reinforced melt bead droplets, which are made by continuously feeding powder or wire into a melt pool formed by a laser or electron beam. Each droplet follows the trajectory set by an automated process planner.

The laser deposition process is illustrated in Fig 1. Concentrically arranged nozzles feed metal powder into the laser melt pool. As the substrate is translated in the *x*-direction, overlapping melt bead droplets form the first layer. The substrate is then incrementally lowered in the *z*-direction and a second layer is formed by rastering in the *y*-direction. This sequence of steps is continued until a three-dimensional solid object is created, which is an exact replica of the original CAD model. By this means, fully dense, complex-shape structural and functional parts with internal geometries and overhangs are possible.

Laser engineered net shaping (LENS^{TM}) and laser additive manufacturing (LAM^{SM}) are two commercial laser-based direct deposition processes for metals. LENS^{TM} uses a low-power Nd:YAG laser and fine-particle powder, which produce small (mm or so) melt pools and heat-affected zones (Ref 2). It creates parts with thin walls and fine intricate features, very close to their final dimensions, thus requiring little or no finishing. With LENS^{TM} precision is high, but the build-rate is low, of the order of 0.05 kg/h. Parts made by LENS^{TM} have a high degree of complexity and a relatively smooth surface finish. LENS^{TM} has been used to make tooling with conformal cooling channels for high-volume manufacturing and parts with functionally graded microstructures, e.g., a gear with a tough core and a hard, wear-resistant surface (Ref 3). Such geometries and microstructures are not possible with conventional manufacturing technologies such as metal casting and powder metallurgy.

LAM^{SM} uses a high-power CO_2 laser and coarse-particle powder to form the melt pool, which is relatively large (cm or so), and a heat-affected zone that is substantial (Ref 4). LAM^{SM} creates *near* net-shape parts with thick walls and coarse features, requiring final machining to achieve accurate dimensions and smooth surface finish. Precision is sacrificed during deposition, but the build-rate is high, of the order of 5 kg/h, which is 100 times greater than LENS^{TM}. The advantage of building parts to a near net-shape is to reduce "buy-to-fly," i.e., reduce material usage, machining time, tooling costs, and product realization time. For certain aerospace parts, cost savings of 20–50% are possible when machining of forgings is replaced by layer-by-layer manufacturing.

LENS^{TM} produces small parts, a few centimeters in size. LAM^{SM} produces large parts, a few meters in size. Both processes can produce fully dense, porosity-free parts. The as-deposited LAM^{SM} parts have a rippled or "stair-step"

S.G. Lambrakos and **K.P. Cooper**, Materials Science and Technology Division, Naval Research Laboratory, Washington, DC. Contact e-mail: lambrakos@anvil.nrl.navy.mil.

surface finish, which is typical of most layer-by-layer manufactured products. LAM^{SM} parts are of moderate complexity. Because of their rippled surface finish, however, LAM^{SM} parts require subsequent finish machining.

The electron beam is another source of directed energy for direct deposition of metal. When used with metal wire feed, e-beam processes have advantages such as excellent coupling of the e-beam with metals and little material loss. In the e-beam freeform fabrication (EBF^3) process, metal wire is fed at a constant rate into the melt pool formed on the substrate by the e-beam (Ref 5). The workpiece sits on a stage that is translated in the *x*- and *y*-directions, incrementally lowered in the *z*-direction, and rotated. At present, the EBF^3 system is a modification of an e-beam welding apparatus and is privy to all the control systems available for welding. Similar to laser deposited structures, EBF^3 fabricated structures also have a rippled surface, requiring finish machining.

Direct-deposition-of-metal processes must address the same metallurgical issues as welding processes. For example, microstructures in the heat-affected zone and fusion zone, grain size and orientation, alloy element segregation, and oxidation need extensive study. Surface finish, dimensional accuracy, part distortion, porosity, thermal stress, and thermal cracking are also issues that need detailed study. Melt pool visualization, thermal imaging, and finite element models have been developed to understand microstructural evolution in direct deposited metals (Ref 6). Thermal models have been developed to establish optimal processing windows or process maps and generate process control methods to fabricate parts with good surface finish, good dimensional tolerance, and low residual stress (Ref 7).

Layer-by-layer deposition processes are capable of fabricating metallic parts from a variety of alloys. Stainless steel, tool steel, titanium, rhenium, aluminum, and nickel-based superalloys are some of the alloys that have been successfully processed. Applications in the automotive, energy, aerospace, defense, and biomedical industries are targeted. Prototype parts are routinely made. The manufacture of load-bearing and functional parts, however, is faced with technical and economic hurdles. As layer-by-layer manufacturing matures, however, i.e., this process becomes affordable and its technical problems are solved, more applications should be forthcoming. For reliability in manufacturing and consistency in part performance, direct deposition of metal with precise closed loop process control must be developed. For process control, it is important to understand the evolution of the microstructure and the nature and magnitude of the thermal fields.

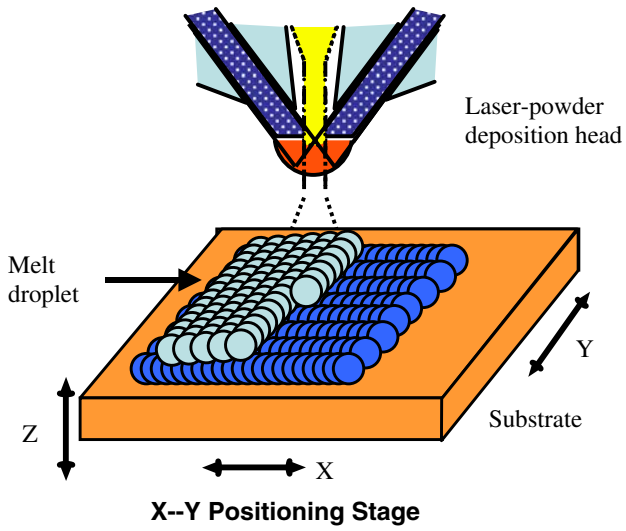

Fig. 1 Schematic representation of laser deposition process showing overlapping of melt bead droplets to build a three-dimensional metallic structure

2. Microstructural Features of Deposits

In this section, some general microstructural features of structures that are fabricated by layer-by-layer deposition processes are examined. For direct deposition of metallic structures, metal powder or wire is fused onto a workpiece and a part is built layer-by-layer from the bottom up. Direct deposited metallic structures appear as a series of weld beads arranged side by side and one above the other. Examples of the microstructure showing overlapping melt bead droplets are shown in Fig 2.

The microstructure in Fig. 2(a) shows three laser-powder deposited layers, the middle layer being orthogonal to the other two (Ref 8). The microstructure in Fig. 2(b) shows several e-beam-wire deposited layers (Ref 9). In both examples,

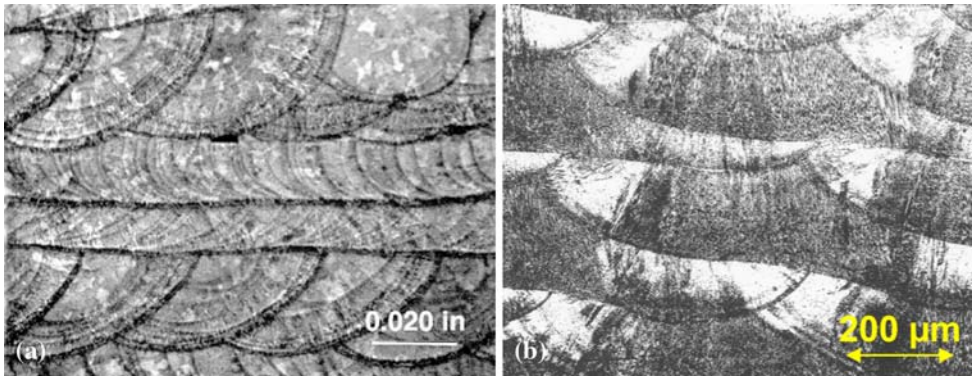

Fig. 2 Examples of microstructure showing overlapping melt bead droplets. (a) Laser-powder deposited (Courtesy: William Hofmeister, Vanderbilt University.) (b) E-beam-wire deposited (Courtesy: Thomas Eagar, MIT)

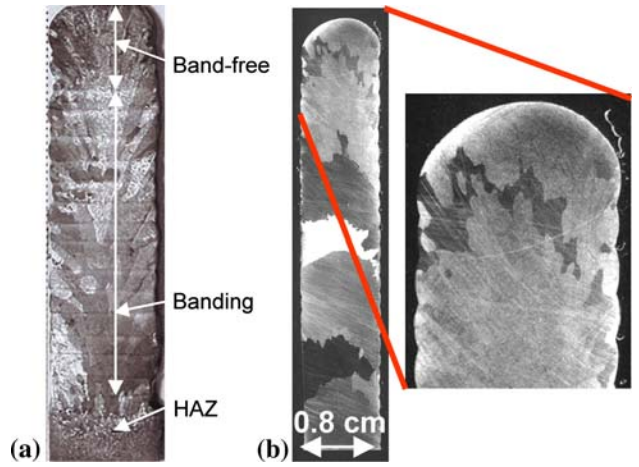

Fig. 3 Microstructures in build direction in LAM^{SM}-fabricated materials. (a) Ti-6Al-4V. (b) Rhenium (Samples courtesy of AeroMet Corp.)

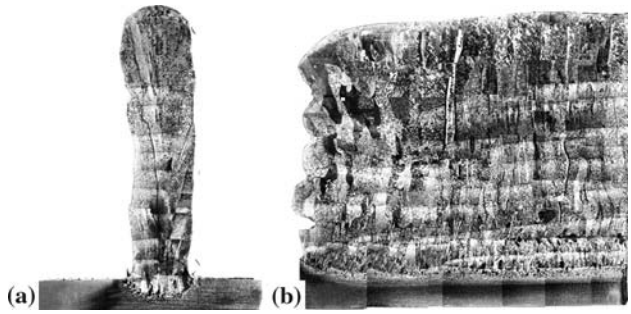

Fig. 4 Microstructures in EBF^3 deposited Ti-6Al-4V. (a) Section perpendicular to translation direction. (b) Section parallel to translation direction (Sample courtesy of NASA Langley Research Center)

hemispherical segregation bands define the melt pool shape. Remelting of previous weld beads brought about by overlapping is evident as is the radial orientation of grain structure within each melt pool. These microstructural features are similar to those obtained in multi-pass welding (Ref 10).

A freeform fabricated rectangular coupon is made by a straight-line build-up process, i.e., depositing metal on a substrate which is translated back and forth. A freeform fabricated cylinder is made by a circular build-up process, i.e., by the depositing of metal on a rotating substrate. The microstructures of the cross sections in the build direction are shown in Fig. 3. Figure 3(a) shows a microstructure in a LAM^{SM} fabricated Ti-6Al-4V rectangular test coupon (Ref 11). The test piece is made up of several layers defined by the ripples on the surface. The surface ripples are remnants of surface tension-driven spherical melt pools. The size and shape of the surface ripples depend upon the surface tension and density of the alloy, and the size of the melt pool and its associated fluid dynamics, all of which depend upon the heat input and temperature distribution, which is a subject for study in itself relative to the direct-problem approach.

The microstructure of the cross section of the coupon shows three distinct regions, heat-affected zone (HAZ) in the substrate, banding in the body of the deposit, and a band-free top layer. Most of the heat is dissipated through the substrate, which is typical of welding processes, and hence, the HAZ has a hemispherical shape. The bands are highlighted by segregation and define the shape of the melt pool. The bands also appear to correspond to the ripples on the surface. The shape of the bands suggests a flat-bottomed weld pool, which is very different from the usual hemispherical shape of a typical weld pool. This suggests that most of the heat transfer in the free formed structure is through the bottom and through previous layers. The band-free top region consists of the last melt bead droplets to solidify. It suggests a spherical melt pool shape, which is several times larger than the band spacing or layer thickness. This means that considerable remelting of the previous layers must have taken place. The grain structure shows elongated and columnar grains that appear to traverse across several bands or layers, suggesting strong epitaxial growth. The columnar grains appear to grow in the build direction but also toward the coupon surface, probably due to convective and radiative heat transfer from the coupon walls.

Shown in Fig. 3(b) are microstructures obtained in a cylinder wall of pure rhenium that was fabricated using LAM^{SM} (Ref 12). The rhenium grain structure is much coarser and less columnar than that in Ti-6Al-4V. The grain size is a few millimeters and the grain boundaries in the growth direction appear faceted. There is some indication of grain orientation in the build direction. The aspect ratio of the grains is small compared to the titanium alloy. The high magnification view of the top of the deposit highlights the surface ripples and the spherical shape of the last weld bead or layer to form, which is similar to that observed in the titanium sample.

The width of the Ti-6Al-4V sample wall is 1.5 cm, while that of the rhenium sample is 0.8 cm. Since each layer is a single pass of melt bead droplets, the width of the melt pool is also 0.8 cm. The grain size and morphology differences between the two metals are best explained by the vast differences in their melting points as well as the fact that one is an alloy and the other is a pure metal. The melt pool shape in rhenium could not be determined because, being a pure metal, the macro etch revealed the grain structure, but not the segregation bands that would define the shape of the melt bead.

Shown in Fig. 4 are microstructures obtained in a Ti-6Al-4V alloy rectangular coupon deposited by the EBF^3 process using single pass welds. Figure 4(a) shows a section perpendicular to the sample translation direction. The coupon is approximately a centimeter thick. Figure 4(b) shows a section parallel to the sample translation direction. Surface ripples, segregation bands, and grain orientation in the build direction are similar to those found in laser-deposited Ti-6Al-4V material. Grain growth is epitaxial, and some of the grains appear to traverse across several segregation bands, which define individual layers. One grain in Fig. 4(a) appears to extend all the way to the top of the deposit. As in the laser-deposited sample in Fig. 3(a), the segregation bands are flat, suggesting a flat-bottomed melt pool and unidirectional heat flow down through the previous layers. Dimensional control in the coupon appears poor because the sample was prepared under less than optimum conditions. These results demonstrate, however, the viability of EBF^3 as a layer-by-layer fabrication technique.

The inherent complexity of layer-by-layer deposition processes demonstrated by the above examples of various fabrication techniques establishes that modeling of heat transfer

in such processes represents a relatively difficult task. This is expected to be especially the case when modeling such processes using basic theory or modeling based on first principles. That is to say, when modeling layer-by-layer deposition processes using the direct-problem approach. A general approach to overcoming modeling difficulties associated with the inherent complexity of energy deposition processes is the inverse-problem approach. Accordingly, an algorithm is presented here for inverse modeling of unsteady heat conduction within structures that are fabricated using layer-by-layer deposition processes. A significant aspect of the structure of this algorithm is that it is based on a mathematical formulation having a relatively small number of adjustable parameters. Methods of inverse analysis, in contrast to analysis methods based on the direct-problem approach, are characterized by many properties that follow directly from the fact that inverse methods are data driven as well as model driven (Ref 13, 14). Principal among these properties is the fact that relatively complex and highly nonlinear systems can be represented accurately by means of model representations characterized by small numbers of parameters. In many cases the errors that are introduced by approximations underlying an inverse model, and its associated relatively small number of parameters, are in fact compensated for by the characteristics of the data space.

In the following sections, a statement of the specific inverse problem to be considered is presented followed by a derivation of an algorithm characterized by a small number of parameters for inverse modeling of unsteady heat conduction that occurs during layer-by-layer deposition processes. Accordingly, a small number of model parameters provides for convenient and practical optimization of parameter values relative to a given data space consisting of measured temperature values or observations of phase transformations, e.g., solidification. The primary goal of this paper, as in previous studies, however, is the development of an inversion infrastructure that provides advantages relative to all aspects related to its utility, including sensitivity analysis.

During the course of the development that follows, the physical assumptions and mathematical approximations underlying the derivation of the algorithm are elucidated. A discussion is presented of specific aspects of the algorithm within the context and objectives of the general inverse heat transfer problem. Subsequently, the algorithm is applied to the analysis of unsteady heat conduction within a prototype layer-by-layer deposition process. The discussion of the results of this analysis considers their significance relative to sensitivity, boundary effects, and computational complexity. In particular, what physical characteristics of the melt bead droplets are significant for inverse analysis, and accordingly, what characteristics of the calculated temperature field are well posed for inverse modeling. The overall context of this effort concerns investigation of unsteady heat transfer within metal structures that are fabricated using layer-by-layer deposition processes.

3. Process Parameters For Layer-By-Layer Deposition

A list of process parameters for layer-by-layer manufacturing of net-shape metallic parts by direct deposition of metal processes is given in Table 1. These parameters are not very different from those used for laser or e-beam welding, especially, if it involves multi-pass welding. However, in order to obtain tighter dimensional tolerance, reasonable surface finish, and, most important, controlled thermal stress, intelligent control of process parameters is essential. Excessive thermal stress can result in cracking and delamination between layers. Also, manufacturing processes need to be reliable so quality parts can be produced consistently. The goals of layer-by-layer manufacturing are to determine the "build envelope" and to achieve "closed loop process control" to fabricate high quality parts and components for critical applications.

Table 1 Process parameters for direct deposition of metal processes

Process parameters
Laser or e-beam power
• Power density
• Focus
• Effect in z dimension
Powder or wire feed rate
• Focus
• Z range of build
Traverse velocity
Hatch ($x-y$) spacing
Z increment

One way to achieve these goals is to develop methods to determine the thermal fields, temperature histories, and fluid flow fields within the melt pool and the solidified layer. From this analysis, process control algorithms can be determined for specific materials and processes. We employed the inverse-problem approach to determine thermal fields in direct deposition of metal processes.

4. Statement of Inverse Problem

In contrast to the inverse-problem approach, the direct-problem approach involves utilizing models based on first principles or basic theory. The lack of accurate thermo-physical property data of many engineering alloys, especially at high temperature, however, tends to diminish the utility of direct-problem approaches. The inverse-problem approach also uses equations of basic theory. Inverse models, however, are augmented by experimental data such as solidification cross sections, dimensions and shape, top-surface morphology, thermocouple measurements, relative position and spatial character of energy source, energy per distance, and any information related to the temperature history of the deposit. This approach involves constrained parameter optimization.

The inverse problem concerning analysis of physical processes, in general (Ref 15), and the inverse heat transfer problem, in particular (Ref 16), may be stated formally in terms of source functions (or input quantities) and multidimensional fields (output quantities). Other investigators have also focused on various aspects of inverse problems related to heat deposition processes especially as they relate to the determination of heat fluxes via appropriate regularization of their spatial and time distributions (Ref 17). In general, the formulation of a heat conductive system occupying an open

bounded domain Ω with an outer boundary Γ_o and an inner boundary Γ_i involves the parabolic equation

$$\frac{\partial T(\mathbf{x},t)}{\partial t} = \nabla \cdot (\kappa(\mathbf{x},t)\nabla T(\mathbf{x},t)) \text{ in } \Omega \times (0,t_f), \quad \text{(Eq 1a)}$$

with initial condition

$$T(\mathbf{x},0) = T_0(\mathbf{x}) \text{ in } \Omega, \quad \text{(Eq 1b)}$$

and heat flux exchanges through the outer and inner boundaries Γ_o and Γ_i as follows:

$$-\kappa(\mathbf{x},t)\frac{\partial T(\mathbf{x},t)}{\partial n_{\Gamma_o}} = c(\mathbf{x},t)(T(\mathbf{x},t) - T_a(\mathbf{x},t)) \text{ on } \Gamma_0 \times (0,t_f) \quad \text{(Eq 1c)}$$

$$-\kappa(\mathbf{x},t)\frac{\partial T(\mathbf{x},t)}{\partial n_{\Gamma_i}} = q(\mathbf{x},t) \text{ on } \Gamma_i \times (0,t_f). \quad \text{(Eq 1d)}$$

where $\mathbf{x} = (x,y,z)$ is the position vector, n_{Γ_o} and n_{Γ_i} are the normal vectors onto boundaries Γ_o and Γ_i, respectively. The quantities t and t_f are the time and final time, respectively. The quantities $T(\mathbf{x},t) = T(x,y,z,t)$ and $\kappa(\mathbf{x},t) = \kappa(x,y,z,t)$ are the temperature field and diffusivity function, respectively, and $c(\mathbf{x},t) = c(x,y,z,t)$ and $T_a(\mathbf{x},t) = T_a(x,y,z,t)$ are specified functions. The function $q(\mathbf{x},t) = q(x,y,z,t)$ is the heat flux on the inner boundary Γ_i. Determination of the temperature field via the solution of Eq 1(a) to (d) defines the direct initial-boundary value problem. Interest here, however, is focused on that of a formulation of the inverse problem that can be stated as follows: Effectively reconstruct the heat flux field $q(x,y,z,t)$ on the inner boundary Γ_i, and the resulting temperature field $T(x,y,z,t)$ for all time $t \in [0, t_f]$ when the boundary Γ_i is totally or partially inaccessible. In order to reconstruct the heat flux, additional information concerning the temperature $T(x,y,z,t)$ is needed (i.e., known values that have been acquired experimentally) (Ref 15, 17).

In the present analysis the inverse problem is defined in the context of the layer-by-layer deposition as shown schematically in Fig. 1. According to Fig. 1, it is noted that the source function $q(x,y,z,t)$ is to be determined in terms of its volumetric spatial and temporal characteristics. Further, additional information that is needed lies within a data space for analysis of this system that in general consists of (a) measurements of the temperature $T(x,y,z,t)$ at different locations and times on the surface of the structure, e.g., thermocouple measurements, (b) the location of the central point of the source functions $q(x,y,z,t)$ within the volume of the structure, e.g., postmortem melting profiles of the metal within the regions of the melt bead droplets, (c) information concerning the spatial and temporal characteristics of the source functions $q(x,y,z,t)$, i.e., melt bead droplets, and (d) information concerning the thermal diffusivity of the material.

Information concerning the spatial and temporal characteristics of $q(x,y,z,t)$ would in principle include the shapes of solidification boundaries resulting from localized melting. Information concerning the thermal diffusivity of the material would be the average diffusivity for a range of temperatures.

Formulation of an algorithm for inverse modeling of unsteady heat conduction within structures occurring during layer-by-layer deposition processes follows from the different properties associated with deposition of melt bead droplets. These include filter properties, symmetry properties, and optimal sampling for reduction of computational complexity. In what follows, it is shown that the contiguous and sequential activation of elemental energy sources along a linear path within the volume of a conductive region actually introduces physical conditions that permit, mathematically, the introduction of a symmetry cut within the region and along the path of deposition. This symmetry cut intersects the central point of the elemental sources specified by a function $q(x,y,z,t)$. This symmetry cut permits a mapping of the symmetry plane with a locally unbounded domain onto a nonconducting boundary surface of a region of finite thickness, or volume in general. A condition for the accuracy of this mapping is that certain aspect ratios be sufficiently small relative to dominant spatial shape features of the source function $q(x,y,z,t)$. For example, a reasonable aspect ratio can be that of the diameter of the melt bead droplets and the distance of the point of temperature history sampling from that of deposition at the surface of the structure. For unsteady heat deposition within a planar structure of finite thickness, or volume in general, a consistent parametric representation of the time-dependent temperature field is constructed from a set of basis functions $T_k(\hat{x},\hat{x}_k,n\Delta t)$ satisfying Eq 1(a) according to

$$T(x,y,z,t) = T_A + \sum_{k=1}^{N_k}\sum_{n=1}^{N_t} T_k(\hat{x},\hat{x}_k,n\Delta t) \quad \text{(Eq 3)}$$

The vector $\hat{x} = (x,y,z)$ are positions within the structure, and $\hat{x}_k = (x_k,y_k,z_k), k = 1,\ldots,N_k$, are the locations of the elemental heat sources. The quantities Δt and n are the timestep and timestep index, respectively, where the time $t = n\Delta t$. The ambient temperature T_A has the value 25 °C.

5. Algorithm Formulation

In this section the basic mathematical elements underlying the formulation of the algorithm for inverse modeling of layer-by-layer deposition processes are presented. This algorithm is based on the construction of a parametric representation of the time-dependent temperature field in terms of a set of basis functions, i.e., Eq 3, whose trends are consistent with that of the temperature field occurring with the structure of interest. In the case of layer-by-layer depositon processes, reference to example system shown in Fig. 1 through 4 implies that a reasonable set of basis functions are

$$T_k(\hat{x},\hat{x}_k,n\Delta t) = C(\hat{x}_k,n\Delta t)F_k(\hat{x},\hat{x}_k,n\Delta t,\kappa) \quad \text{(Eq 4a)}$$

where

$$F_k(\hat{x},\hat{x}_k,n\Delta t,\kappa) = \frac{1}{(n\Delta t)}\exp\left[-\frac{(x-x_k)^2-(y-y_k)^2}{4\kappa(n\Delta t)}\right] \times \left\{1 + 2\sum_{m=1}^{\infty}\exp\left[-\frac{\kappa m^2\pi^2(n\Delta t)}{l^2}\right] \times \cos\left[\frac{m\pi z}{l}\right]\cos\left[\frac{m\pi z_k}{l}\right]\right\} \quad \text{(Eq 4b)}$$

and the quantity l is the thickness of a planar structure, or where

$$F_k(\hat{x},\hat{x}_k,n\Delta t,\kappa,V_k)=\frac{1}{\sqrt{(n\Delta t)}}\exp\left[-\frac{[x-x_k]^2}{4\kappa(n\Delta t)}\right]\times\left\{1+2\sum_{m=1}^{\infty}\exp\left[-\frac{\kappa m^2\pi^2(n\Delta t)}{a^2}\right]\times\cos\left[\frac{m\pi y}{a}\right]\cos\left[\frac{m\pi y_k}{a}\right]\right\}\times\left\{1+2\sum_{m=1}^{\infty}\exp\left[-\frac{\kappa m^2\pi^2(n\Delta t)}{l^2}\right]\times\cos\left[\frac{m\pi z}{l}\right]\cos\left[\frac{m\pi z_k}{l}\right]\right\} \quad \text{(Eq 4c)}$$

and the quantities a and l specify the cross-sectional dimensions of a structure.

At this point it is necessary to examine the basis functions $T_k(\hat{x},\hat{x}_k,n\Delta t)$ with respect to inverse analysis as defined above in the section "statement of inverse problem," in contrast to modeling based on the direct-problem approach. Accordingly, the goal is construction of the temperature field within regions of interest that are within specified boundary surfaces, which do not necessarily coincide with physical boundaries of the workpiece or structure. Relative to this goal there are specific functional characteristics of the different component factors making up the basis functions defined by Eq 4(a) to (c) that provide the foundation of an algorithm for inverse analysis of layer-by-layer deposition processes. These functional characteristics are with respect to filter and symmetry properties associated with heat transfer that occurs during such processes.

For layer-by-layer deposition processes filter properties are perceived intuitively by the observation that the diffusion of heat within a structure that is being built is insensitive to many of the details associated with specific shape features of a given melt bead droplet and, for many locations within the structure, influences of physical boundaries. These filter properties can be shown rigorously by referring to Eq 4(a) to (c), and by assuming that deposition occurs along a linear path coincident with the x-axis. Given this assumption, it follows that the dominant trend factor of the basis functions Eq 4(a) to (c) is

$$f_t(x)=\exp\left[-\frac{(x-x_k)^2}{4\kappa t}\right] \quad \text{(Eq 5)}$$

Next, taking the spatial Fourier transform $\hat{f}_t(k)$ of Eq 5, one obtains

$$\hat{f}_t(k)=\int_{-\infty}^{\infty}f_t(x)\exp(-2\pi ikx)dx=\sqrt{\frac{\pi}{\alpha}}\exp\left[-\frac{\pi^2k^2}{\alpha}\right] \quad \text{(Eq 6a)}$$

where

$$\alpha=\frac{1}{4\kappa(n\Delta t)} \quad \text{(Eq 6b)}$$

The form of $\hat{f}_t(k)$ is within the class of low-pass spatial filter functions whose range of filtered spatial modes k increases with time t. Referring to Eq 4(a) to (c), this filtering is with respect to spatial modes associated with both the heat source function $q(x,y,z,t)$, or equivalently, the spatial distribution of the coefficients $C(\hat{x}_k,n\Delta t)$, and factors making up the functions $F_k(\hat{x},\hat{x}_k,n\Delta t,\kappa)$ that represent boundaries that are nonconducting. The filter properties that are based on Eq 6(a) and (b) establish conditions that provide for parameter reduction with respect to representation of spatial features associated with both melt bead droplets and boundaries.

For layer-by-layer deposition processes certain symmetry properties follow directly from their nature. It is a mathematical property of contiguous linear distributions of discrete elemental heat sources that there manifest two perpendicular symmetry planes, which are parallel to the deposition path, across which there is no conduction of heat. The property establishes conditions that provide for the construction mappings from locally unboundered conductive regions onto equivalent nonconducting boundaries.

The filter and symmetry properties associated with layer-by-layer deposition processes are significant in that the general complexity of an algorithm for inverse modeling of such processes can be reduced. Relative to this point, insight can be obtained by considering the mathematical formalism of algorithm complexity theory. Accordingly, the complexity of an algorithm can be expressed in terms of its computational cost N_{lbl}, which represents the number of operations required for its implementation. For layer-by-layer deposition processes this quantity may be decomposed into different contributions such that

$$N_{\mathrm{lbl}}=N_{\mathrm{d}}N_{\mathrm{t}}N_xN_yN_z \quad \text{(Eq 7a)}$$

where

$$N_{\mathrm{d}}=N_{\mathrm{S}}N_{\mathrm{q}} \quad \text{(Eq 7b)}$$

and

$$N_{\mathrm{q}}=N_{\mathrm{V}}N_{\mathrm{B}} \quad \text{(Eq 7c)}$$

The different factors contributing to the computational cost N_{lbl}, Eq 7(a) to (c), are as follows. The quantities N_{d} and N_{t} are the number of droplets and discrete time steps, respectively, $N_xN_yN_z$ is the size of the system in terms of number of discrete volume elements, N_{S} and N_{q} are the number of elemental heat sources per droplet and the number of operations per heat source element, respectively. The number of operations N_{q} is in principle decomposable, i.e., Eq 7(c), into the number of operations associated with volumetric heat transfer N_V and that number associated with weighting of heat transfer by the presence of nonconducting boundaries N_{B} (see Eq 4b and c).

Systematic reduction of algorithm complexity for inverse modeling of layer-by-layer deposition processes is discussed, as well as demonstrated, within the context the prototype analysis that follows. Before proceeding, it is significant to note that the filtering properties impose conditions such that $N_{\mathrm{S}}=1$ and that the calculation of temperature histories at a finite number of sample points provides a significant reduction in size of simulations in that essentially $N_xN_yN_z=1$.

6. Prototype Analysis

In this section a prototype analysis is presented that demonstrates application of the algorithm to layer-by-layer deposition processes and provides for an examination of mathematical properties underlying the algorithm formulation. The prototype system is that of the freeform fabrication of a

Table 2 Model parameters used to determine thermal fields in direct deposition processes

Model parameters
Material: Steel
Diffusivity: $\kappa = 2.5 \times 10^{-5}$ m^2/s
Timestep: $\Delta t = 0.001$ s
Drop deposited every 20 timesteps
18 drops per layer, 4 layers
Energy content of each drop: $C(\hat{x}_k, n\Delta t) = 25.0$
Volume of each drop = $(10\ \Delta l) \times (10\ \Delta l) \times (20\ \Delta l)$ where $\Delta l = 1.425 \times 10^{-4}$ m

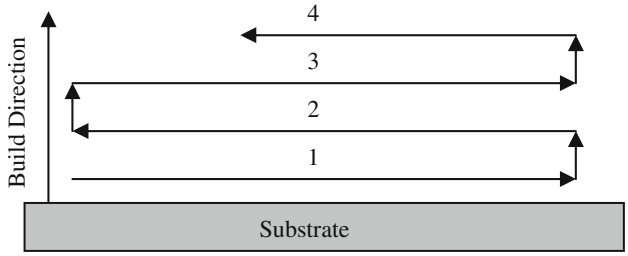

Fig. 5 Schematic representation of layer-by-layer fabrication scheme assumed for calculating thermal fields

rectangular coupon similar to those shown in Fig. 3 and 4 for a system whose thermal diffusivity is within the range of steel. The algorithm formulation is in terms of basis functions that are solutions to the heat conduction equation Eq 3, filter and symmetry properties associated with layer-by-layer deposition of droplets, and global constraint conditions on the deposition rate of mass and energy. Accordingly, a surface distribution of discrete energy sources whose strengths are assigned by the values of the coefficients $C(\hat{x}_k, n\Delta t)$ defined in Eq 4(a) are numerically integrated at each time step. Each of the discrete energy sources represents a discrete liquid metal droplet of a given volume. The translation speed of the sample relative to the point of liquid metal deposition is assigned implicitly through the time dependence and relative locations of the discrete energy sources, $C(\hat{x}_k, n\Delta t)$. That is to say, a certain number of drops per layer and a certain number of layers as a function of time are specified. The model parameters used for the prototype analysis are listed in Table 2. For purposes of this analysis, the basis functions given by Eq 4(b) are adopted for calculation of the temperature field. These functions are solutions to the heat conduction equation for a temperature independent diffusivity and nonconducting boundaries on two surfaces that are separated by a distance l, which will correspond to the thickness of the coupon to be fabricated. As will be demonstrated, other nonconducting boundary conditions are imposed as a result of symmetry conditions that follow from the linear contiguous distribution of energy sources. At the edges of the rectangular coupon, there is no heat transfer into the ambient environment. This is a realistic assumption since conductive heat transfer in these processes is greater than radiative heat transfer. It follows that a simulation that examines fabrication of an entire rectangular coupon should adopt the basis functions given by Eq 4(c) for calculation of the temperature field. Our present analysis, however, examines the unsteady heat transfer at a relatively localized region within the coupon sample and thus adopts the basis functions Eq 4(b). This is sufficient for the purpose of examining the application features and properties of the algorithm. The purpose of the present calculations is to represent parametrically heat conduction through the previous deposited layers and through trailing solidified layers.

A constraint condition imposed for the temperature field calculations is the spatial location of the liquid-solid interface defined by the alloy liquidus temperature, which for the present analysis is chosen to be 1430 °C, in that the thermal diffusity adopted is characteristic steel. Accordingly, the values assigned to the coefficients $C(\hat{x}_k, n\Delta t)$ were such that the average temperature of each discrete droplet was within the range of liquid metal. It is significant to note that other constraint conditions such as melt pool dimensions and measurements of temperature via thermocouples can be adopted for assigning values to the coefficients $C(\hat{x}_k, n\Delta t)$. In the present prototype system the layers are deposited one on top of the other by traversing the passes in a zig-zag fashion as shown schematically in Fig. 5.

Consistent with the filter properties associated with thermal diffusion, each melt bead droplet can be represented by a cube. This follows in that the filtering of fine spatial structure due to the dominant trend factor Eq 5 implies that the temperature field is insensitive to details of the shape of the melt bead droplet. It is significant to note, however, that the temperature field is sensitive to the spatial distribution of droplets.

Shown in Fig. 6 is the time evolution of a region of the prototype coupon specified by the model parameters given in Table 2 and the deposition scheme shown in Fig. 5. Each of the subfigures in Fig. 6 consists of three two-dimensional slices of the calculated three-dimensional temperature field. One slice is that of a face of the coupon, which is parallel to the build direction (the largest region); another slice is that at the interface between the coupon and substrate upon which the deposition occurs; and another slice is parallel to the build direction and through the thickness of the coupon.

At this stage the evolution of the unsteady temperature field shown in Fig. 6 is examined for the purpose of better understanding the characteristics of the algorithm for its application to inverse analysis of layer-by-layer deposition processes. Before proceeding it should be noted that the calculation of the temperature field over two-dimensional slices is for the purpose of examining properties of the algorithm. In practice the temperature field should be determined at a finite number of sample points thus significantly reducing the complexity of the algorithm such that its computational cost scales only as the number of droplets, i.e., N_d in Eq 7(a). This is demonstrated below. Proceeding, the structure of the temperature field associated with an individual droplet, i.e., Fig. 6(a), is examined. Referring to this figure, it is to be noted that the symmetry properties associated with a point source are equivalent to those of a nonconducting top surface boundary. One is therefore able to adopt Eq 4(a) to (c) for the representation of melt bead droplets, without the need of expending computational cost for the inclusion of top surface boundary influences. This property, which provides for equivalent mappings between symmetry cuts within energy source distributions and nonconducting boundaries, was also examined in reference (Ref 18) for inverse analysis of heat transfer within cylindrical structures. Referring again to Fig. 6, one notes the temperature distribution within the neighborhood of an individual droplet for a time period corresponding to the duration of its deposit. This temperature distribution, and the associated local time evolution of the solid-liquid interface, represents one of the primary

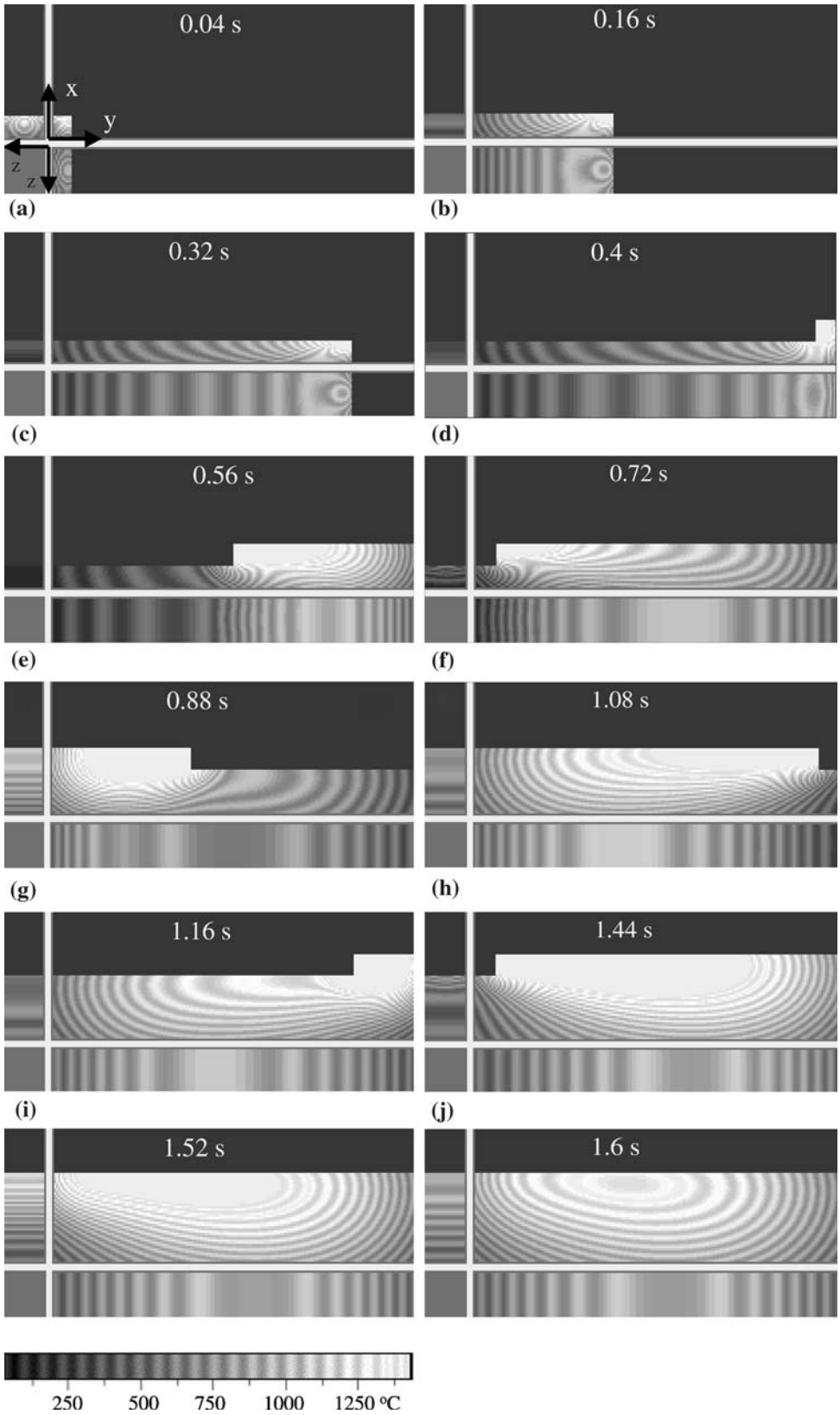

Fig. 6 Spatial and time evolution of temperature field within a localized region of a prototype coupon specified by the model parameters given in Table 2

constraints on the calculated temperature field. The local temperature distribution of an individual droplet provides for the implicit specification of the rate of energy deposition into the system.

Next, the temperature field shown in Fig. 6(b) and (c) is examined. Referring to these figures, it can be observed that the same symmetry properties associated with a point source, which impose nonconducting boundary conditions at the

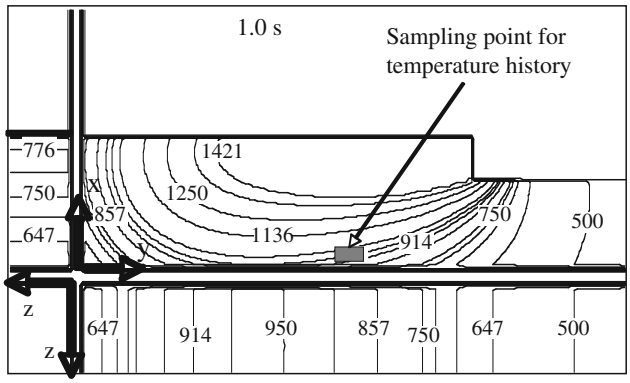

Fig. 7 Sampling point for calculation of temperature history

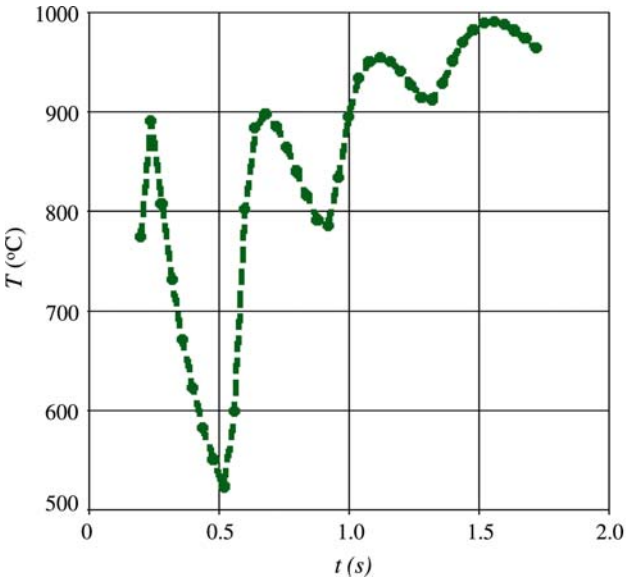

Fig. 8 Temperature history at sampling point indicated in Fig. 7

surface, are extendable to a contiguous linear distribution of sources. Referring to Fig. 6(d) through (j), it is also observed that these symmetry properties are extendable to subsequent layers. That is to say, for each of the individual layers, the trend of the unsteady temperature field is consistent with a nonconduction top surface and windage due to the relative motion of droplet deposition and substrate.

Finally, the temperature field shown in Fig. 6(i) and (j) is examined. The temperature fields shown in these figures are for the cooling period following completion of the droplets deposition sequence. Again, it can be observed that the cooling trend is consistent with a nonconduction boundary located at the top surface of the last layer to be deposited.

The specific aspect of the algorithm, in terms of numerical analysis, which provides for consistent boundary conditions via symmetry properties, thus permitting symmetry cuts, is that the model system comprises a contiguous distribution of active heat sources. This numerical analytical property has the consequence that, at each timestep, the computational cost of the algorithm must scale as the numbers of sources. Therefore, application of the algorithm is more well posed if individual sampling points of the temperature history are selected for calculation. In particular, the temperature histories in the heat-affected zones would be important to understand microstructural evolution in these critical regions, where cracking and delamination are possible. Microstructure dictates mechanical properties, which can mean that the success or failure of using the layer-by-layer fabrication approach to making parts depends upon the production of the right microstructure. Shown in Fig. 7 is an example of a sampling point for the prototype system considered here. Shown in Fig. 8 is the temperature history calculated at this point. Referring to Fig. 8, the following observation can be made. Notably the temperature increases as the layers are built one on top of the other. This follows from the fact that the new layers are continuously deposited on hotter previous layers.

7. Conclusion

Layer-by-layer fabrication of net-shape metallic structures has many advantages. It can respond to rapid changes in part design and provide rapid turnaround time. For direct deposition of metals to be successful as a manufacturing technology, the essentially cast microstructure, similar to that obtained in welding, must demonstrate mechanical properties superior to those obtained in conventionally produced parts. Due to somewhat rapid solidification, the scale of the microstructure is generally finer than in bulk castings and higher yield strength values have been reported. However, a thorough microstructural evaluation of the fabricated part and mechanical properties parallel and perpendicular to the build direction must be performed in order to make the part acceptable to industry. Strong grain orientation in the build direction, as observed in e-beam deposited Ti-6Al-4V, will result in a greater degree of anisotropy in mechanical behavior and is to be avoided. The success of direct deposition of metal processes will depend upon the degree of reliability of the manufacturing technology. For this it is important to develop thermal field models and then relate them to process control in order to produce high quality parts. The algorithm presented here should serve to demonstrate the advantages of the inverse-problem approach for modeling thermal fields occurring during layer-by-layer deposition processes and addressing issues related to the sensitivity of layer-by-layer deposited structures to changes in process parameters, such as reversal of the direction of traverse and changes in boundary conditions. For such sensitivity analyses, further study, which would include microstructure correlation and algorithm development, is required.

Acknowledgments

We would like to thank the many scientists involved in layer-by-layer manufacturing research for sharing their results and the Office of Naval Research for its support.

References

1. K.P. Cooper, Layered Manufacturing: Challenges and Opportunities, *Mat. Res. Soc. Symp. Proc.*, 2003, **758**, p LL141
2. M.L. Griffith, D.M. Keicher, and C.L. Atwood, Fabrication of Metallic Components using Laser Engineered Net Shaping (LENS), *Proc. of SFF Symposium*, University of Texas-Austin, Austin, TX, 1996, p 125

3. P. Chavez, From the Inside Out: The LENS^{TM} Process is Fueling a Paradigm Shift in Modern Manufacturing Applications, *Technical Brief*, Optomec, Inc., 2000
4. F.G. Arcella and F.H. Froes, Producing Titanium Aerospace Components from Powder Using Laser Forming, *JOM*, 2000, **52**(5), p 28
5. K.M.B. Taminger, R.A. Hafley, and D.L. Dicus, Solid Freeform Fabrication: An Enabling Technology for Future Space Missions, *Proceeding of the 2002 International Conference on Metal Powder Deposition for Rapid Manufacturing*, MPIF, Princeton, NJ, 2002, p 51
6. W. Hofmeister, M. Wert, J. Smugeresky, J.A. Philliber, and M. Griffith, M. Ensz, Investigating Solidification with the Laser-Engineered Net Shaping (LENSTM) Process, *JOM-e*, 1999, **51**(7)
7. J. Beuth and N. Klingbeil, The Role of Process Variables in Laser-Based Direct Metal Solid Freeform Fabrication, *JOM*, 2001, **53**(9), p 36
8. W. Hofmiester, Vanderbilt University, Private Communication, 2004
9. D. Dave, J. Matz, and T.W. Eagar, Electron Beam Solid Freeform Fabrication of Metal Parts, *Proceeding of SFF Symposium*, University of Texas-Austin, Austin, TX, 1995, p 64
10. D.W. Moon, S.G. Lambrakos, R.J. Wong, and E.A. Metzbower, Temperature, Macrostructure and Hardness in High Strength Low Alloy Steel Welds, *Sci. Tech. Weld. Join.*, 2003, **8**(5), p 1
11. S.M. Kelly, S.L. Kampe, and C.R. Crowe, Heat Treatment, Micrographic Examination, and Thermal Modeling of Laser Formed Ti-6Al-4V, *Proceeding of Solid Freeform and Additive Fabrication*, Vol. 625, MRS, Warrendale, PA, 2000
12. K.P. Cooper, F.G. Arcella, and H.N. Jones, Rapid Prototyping of Materials, *Proceeding of TMS Fall Meeting*, TMS, Warrendale, PA, 2002, p 119
13. J. Michopoulos and S. Lambrakos, On the Fundamental Tautology of Validating Data-Driven Models and Simulations, *Int. Conf. Comput. Sci.*, 2005, **2**, p 738–745
14. J.G. Michopoulos and S.G. Lambrakos, Underling Issues Associated with Validation and Verification of Dynamic Data Driven Simulation, L.F. Perrone, F. P. Wieland, J. Liu, B. G. Lawson, D. M. Nicol, and R. M. Fujimoto, Eds., *Proceedings of the 2006 Winter Simulation Conference*, December 3–6, 2006, Monterey CA, CD-ROM, ISBN 1-4244-0501-7, IEEE Catalog Nu. 06CH37826
15. A. Kirsch, *An Introduction to the Mathematical Theory of Inverse Problems*. Springer Verlag, New York, 1996
16. S.G. Lambrakos and J.O. Milewski, Analysis of Processes Involving Heat Deposition using Constrained Optimization, *Sci. Technol. Weld. Join.*, 2002, **7**(3), p 137
17. J. Xie and J. Zou, Numerical Reconstruction of Heat Fluxes, *SIAM J. Numer. Anal.*, 2005, **43**(4), p 1504–1535
18. S.G. Lambrakos, J.G. Michopoulos, H.N. Jones, and C.N. Boyer, Inverse Analysis of Heat Conduction in Hollow Cylinders with Asymmetric Source Distributions, *JMEP.* doi:10.1007/s11665-007-9197-x